Asymmetric Magnetic Relaxation Behaviour of Domains and Domain Walls Observed Through the FeRh First-Order Metamagnetic Phase Transition

Jamie R. Massey,[1,*] Rowan C. Temple,[1] Trevor P. Almeida,[2] Ray Lamb,[3] Nicolas A. Peters,[1,4] Richard P. Campion,[5] Raymond Fan,[6] Damien McGrouther,[2] Stephen McVitie,[2] Paul Steadman,[6] and Christopher H. Marrows[1,†]

[1]*School of Physics and Astronomy, University of Leeds, Leeds LS2 9JT, United Kingdom.*

[2]*SUPA, School of Physics and Astronomy, University of Glasgow, Glasgow, G12 8QQ, United Kingdom.*

[3]*School of Physics and Astronomy, University of Glasgow, Glasgow, G12 8QQ, United Kingdom.*

[4]*School of Electronic and Electrical Engineering, University of Leeds, Leeds, LS2 9JT, United Kingdom.*

[5]*School of Physics and Astronomy, University of Nottingham, Nottingham, NG7 2RD, United Kingdom.*

[6]*Diamond Light Source, Chilton, Didcot, OX11 0DE, United Kingdom.*

[*] jamie.massey@psi.ch

[†] c.h.marrows@leeds.ac.uk

CORRECTION OF TEMPERATURE DUE TO APPLIED FIELD

The transition temperature, T_{T}, of the metamagnetic phase transition in FeRh is sensitive to the application of external magnetic field, H_{Ext} [1, 2]. As such, when comparing between measurement performed whilst a magnetic field is applied to those performed in the absence of an external magnetic field, it is necessary to correct the temperature of the measurements in which a field is applied. This corrected temperature is known as the effective temperature, T_{Eff}, and is defined as the temperature at which the same magnetization is expected in the absence of external field [2]. The formula used for its calculation is given by,

$$T_{\mathrm{Eff}} = T_0 - \frac{dT_{\mathrm{T}}}{d(\mu_0 H_{\mathrm{Ext}})}\mu_0 H_{\mathrm{Ext}}, \tag{1}$$

where T_0 is the real sample temperature, μ_0 is the permeability of free space and $dT_{\mathrm{T}}/d(\mu_0 H_{\mathrm{Ext}}$ is the rate of change of the T_{T} with $\mu_0 H_{\mathrm{Ext}}$. All the temperature dependent behaviour shown in the main paper has been corrected in this way.

The dependence of the transition upon varying magnetic field values can be seen by the points in Fig. 1(a). This figure shows the temperature derivative of the magnetization dM/dT for a series of field values, where the position of the peak in dM/dT clearly decreases in temperature with increasing field. The value of T_{T} is extracted by fitting a Gaussian curve to dM/dT [1], which can be seen by the dashed and solid lines in this figure for measurements performed when cooling and heating, respectively. The extracted values of T_{T} are shown against their respective value of $\mu_0 H_{\mathrm{Ext}}$ for both the heating and cooling branches in Fig. 1(b). The linear fit here is used to extract $dT_{\mathrm{T}}/d(\mu_0 H_{\mathrm{Ext}})$ and also the transition midpoint at zero field, T_{M}, as the absiccsa intercept. Values extracted for these measurements are shown in Table I.

TABLE I. Results of linear fits to the dependence on T_{T} on $\mu_0 H_{\mathrm{Ext}}$.

	$\frac{dT_{\mathrm{T}}}{d(\mu_0 H_{\mathrm{Ext}})}$ (K T^{-1})	T_{M} (K)
Heating	$-(7.99 \pm 0.02)$	376.85 ± 0.02
Cooling	$-(8.76 \pm 0.03)$	351.47 ± 0.03

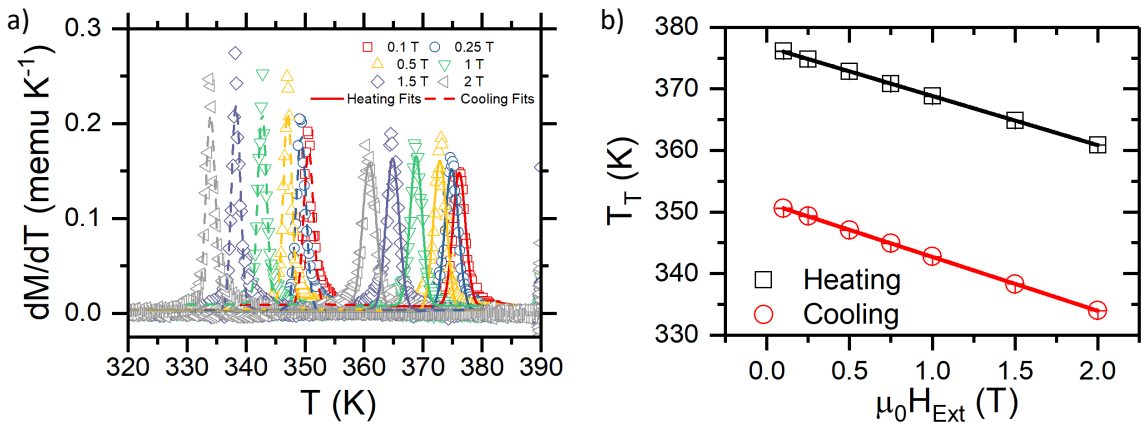

FIG. 1. Dependence of the transition temperature, T_{T}, on external magnetic field. Panel (a) shows the dependence of the derivative of the magnetization, dM/dT, against T for measurements performed in various external magnetic field strengths (points). The solid and dashed lines in this figure are Gaussian fits to the data performed when heating and cooling, respectively. Panel (b) shows the value of the extracted values of T_{T} against the external magnetic field in which the measurements was performed. The linear fit here is used to extract $dT_{\mathrm{T}}/d(\mu_0 H_{\mathrm{Ext}})$ and the transition midpoint at zero field, T_{M}.

X-RAY ABSORPTION SPECTROSCOPY RESULTS

The location of the Fe L_3 resonance edge was identified using X-Ray absorption spectroscopy. To achieve this an energy scan from 690 to 730 eV was performed using both helicities of circular light and both polarizations of linear light (I^+, I^-) and calculating the dichroism, D, using,

$$D = \frac{I^+ - I^-}{I^+ + I^-}. \tag{2}$$

The results for both circular (black solid line) and linear (red solid line) light for scans performed at 400 K are shown in Fig. 2. The presence of dichroism is clearly evident around 707 eV for both dichroism types here.

Also shown on this figure is the positions of the beam energy (dashed lines) that was used in each of the three beamtimes that made up the data presented in the main paper. To make this easier to see, a close up of the energy scan between 705 and 710 eV is shown in Fig. 2(b). Beamtimes 1 and 2 focussed on measurements performed using XMCD so should be judged against the black solid line. Whilst the XMLD measurements were all performed

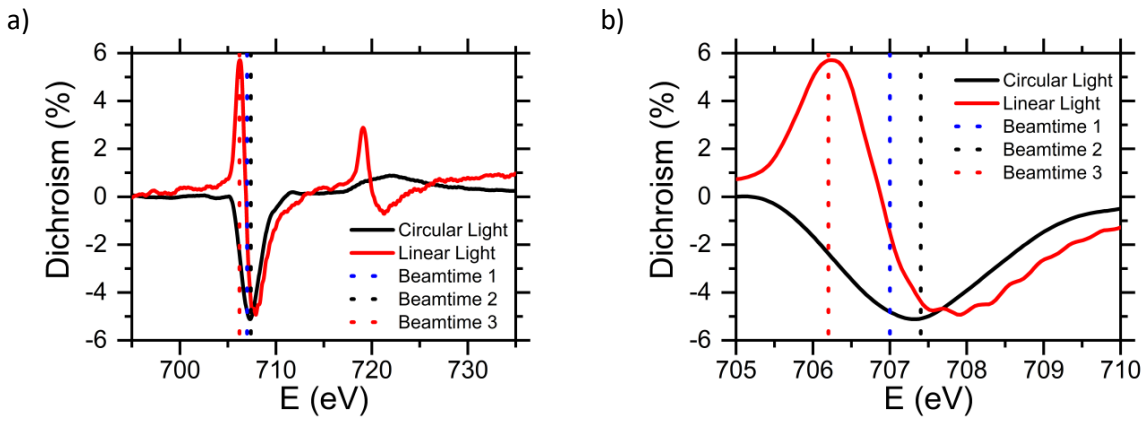

FIG. 2. X-ray absorption spectroscopy results. (a) The value of D against beam energy for both linearly (solid black line) and circularly (solid red line) polarized light taken at 400 K. The dashed lines here show the position of the beam energy used in each of the three beamtimes that make up the XPCS results. (b) a close up of the scan shown in (a) between 705 and 710 eV. Beamtimes 1 and 2 focussed on measurements performed using XMCD so should be judged against the black solid line. Whilst the XMLD measurements were all performed in the 3rd beamtime and so should be compared to the red solid line.

in the 3rd beamtime and so should be compared to the red solid line.

DEMONSTRATION OF RESONANT MAGNETIC SMALL ANGLE SCATTERING

Evidence for the presence of resonant magnetic small angle scattering can be seen in panels (a)-(d) of Fig. 3. These images are examples of those taken with the beam energy both off (panels (a) and (c)) and on (panels (b) and (d)) the Fe L_3 resonance for images taken using circularly (panels (a) and (b)) and linearly (panels (c) and (d)) polarized light. These images are taken using the protocol outlined in the methods section of the main document. Both images taken with beam energies away from the Fe L_3 edge show no appreciable scattering of any kind, whilst those taken on the Fe L_3 edge clearly show a small angle scattering ring with speckle features. The resonant enhancement of the scattering proves that it originates from magnetic order within the sample. The presence of speckle indicates the presence of a disordered magnetic structure, which is consistent with the expected magnetic domain structure at this point in the transition [3, 4].

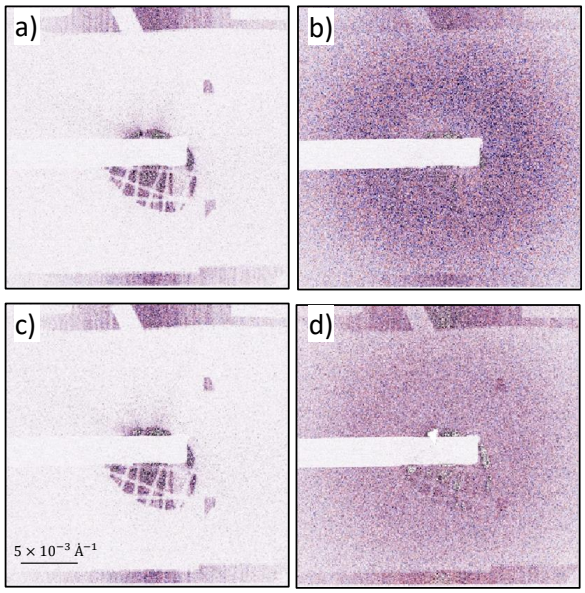

FIG. 3. Transmission RMSAXS patterns. (a) Image taken with a beam energy of 690 eV–off-resonance–at 400 K using circularly polarized light, showing no appreciable scattering. (b) Image taken on the Fe L_3 resonance edge using circularly polarized light, showing a clear SAXS ring with speckle. Equivalent images for linearly polarized light are shown in panels (c) and (d). In all four images the shadow cast by the beamstop is visible as a white rectangle on the left, and the pinhole and crossed TEM grids are visible in the centre of each image.

BEHAVIOUR OF THE SPECKLE AMPLITUDE AND MIXING FREQUENCY

The behaviour of the speckle amplitude, A, and the time constant associated with the mixing frequency $2\pi/\omega$, extracted from the fits of the stretched exponential model to the g_2 curves are shown against temperature for both the XMCD and XMLD measurements are shown in Fig. 4.

For the XMCD measurements, the extracted value of A, shown in Fig. 4(a), decreases with temperature from $\sim 0.2 \rightarrow \sim 0$ when cooling and increases between the same values when heating. It is worth noting here that the values of each quantity extracted from measurements using only a single helicity are used except for values of A, as this was significantly lower than values extracted from the measurements where both helicities were available. This behaviour consistent with the changes in the volume of FM domains through the transition. The values of A extracted from the XMLD measurements, shown in Fig. 4(c), shows a

quasi-linear increase between $A \sim 0.01-0.1$ with decreasing temperature when cooling. The behaviour when heating for the XMLD measurements is consistent at around $A \sim 0.06$ for measurements performed below the transition midpoint (dashed lines). For measurements performed for $T > T_{\mathrm{M}}$ when heating, A decreases with temperature from ~ 0.06, reaching ~ 0.05 at 400 K.

The behaviour of the time constant associated with the mixing frequency, $2\pi/\omega$, extracted from the XMCD measurements is shown in Fig. 4(b). When cooling $2\pi/\omega$ decreases from 1.25 to 0.5 hours. When heating, for measurements performed below T_{M}, there appears to be a large scatter in the data which extracted values ranging between 1.5 and 0.25 hours. For measurements where $T > T_{\mathrm{M}}$ the value of $2\pi/\omega$ extracted decreases from ~ 1 to ~ 0.5 hours. The variations in $2\pi/\omega$ do not follow the behaviour of λ shown in the main paper, which suggests that both the charge and magnetic components of the scattering from the FM regions exhibit fluctuations. The reason for this unknown at this stage.

The time constant extracted for the XMLD measurements appears to be largely invariant at around ~ 0.75 hours for the measurements ranges here with no clear trend for the measurements performed whilst heating. The XMLD measurements taken when cooling, however, appear to dip at the transition midpoint from ~ 1.5 hours to ~ 0.8 hours. The variations in the data here appear to follow the behaviour of λ shown in the main paper, suggesting that the charge fluctuations probed with XMLD are constant.

DEPENDENCE OF THE DYNAMIC BEHAVIOUR ON THE EXTRACTED LENGTH-SCALE

As explained in the main body of this work, the dynamic behaviour of the system can sometimes be reliant upon the length scales present in the system [5–7], particularly in the case of critical scaling. The values of the stretching exponent, β, and the relaxation time, λ, extracted from the analysis of the temporal correlation functions are shown in Fig. 5 against the extracted length scale, d, for all measurements. Measurements performed using XMCD are shown in panels (a) and (b), whilst measurements performed using XMLD are shown in panels (c) and (d). It is clear from this figure that there is no real correlation or dependence of either of the quantities governing the dynamic behaviour upon d. Therefore, we are unable to reconcile the changes in the dynamic behaviour seen in this work with the

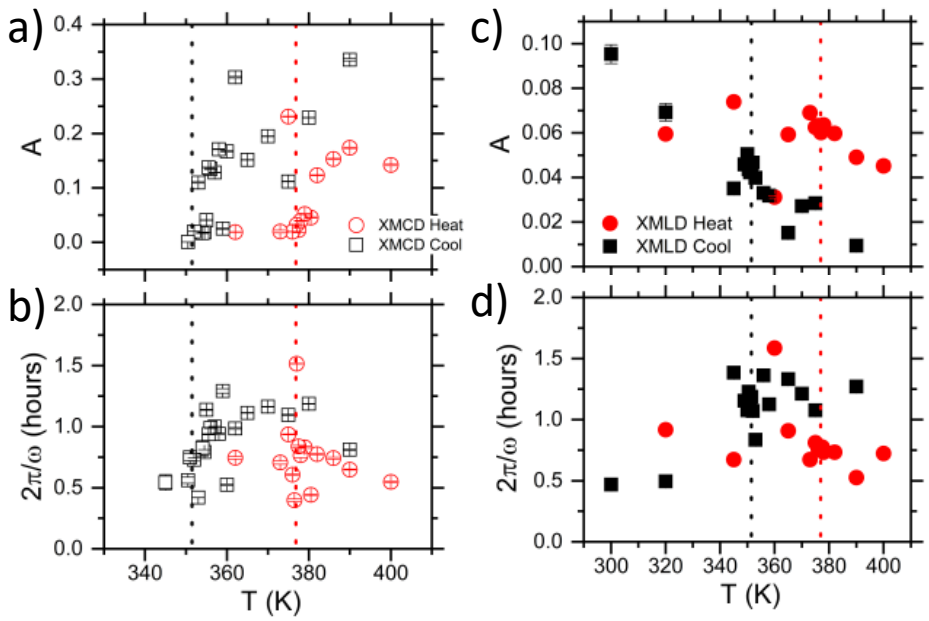

FIG. 4. Temperature dependence of the speckle amplitude, A, and time constant associated with the mixing frequency, $2\pi/\omega$ for all measurements. (a) and (c) show the temperature dependence of A for all measurements extracted for the fits of the stretched exponent model to the g_2 curves for the XMCD and XMLD measurements, respectively. (b) and (d) show the extracted values of $2\pi/\omega$ for the XMCD and XMLD measurements. The dashed lines show the position of the transition midpoint measured using magnetometry.

changes in the nature of the scatterer through the transition.

MAGNETIC VISCOSITY MEASURED USING A MAGNETOMETER UNDER VARYING CONDITIONS

The results of the magnetic viscosity measurements performed using a magnetometer presented in the main body of the text are those that best replicate the conditions used in the XPCS experiment with regards to the temperature sweep rate. In these measurements a field is required to prevent artefacts being introduced into the data. Also performed were measurements of the same sample that use a temperature sweep rate of 10 K min^{-1} with no external magnetic field applied. These are found to have two regimes of development as

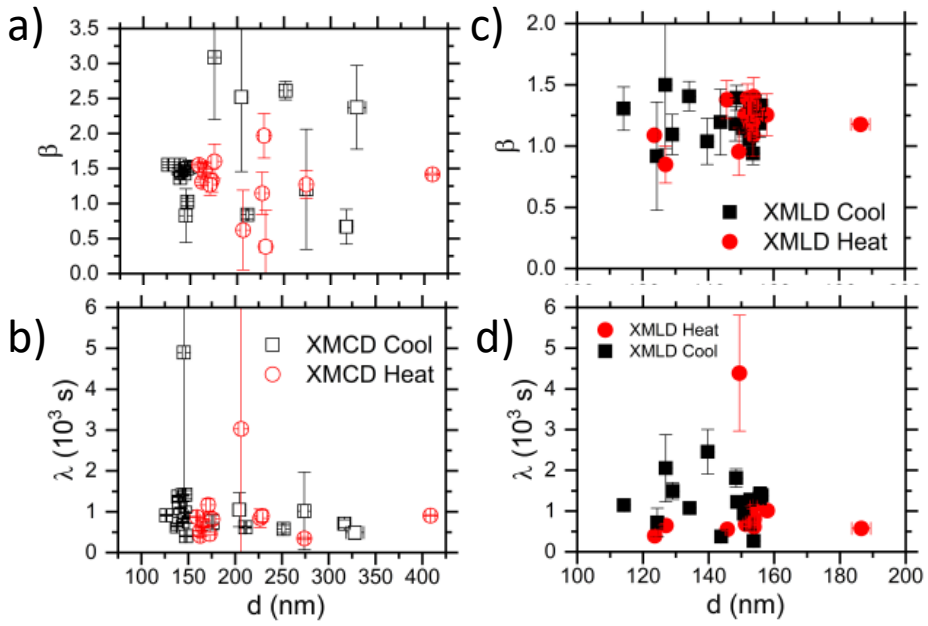

FIG. 5. Dependence of the dynamic behaviour on extracted lengthscale. Panels (a) and (b) show dependence of the values of the stretching exponent, β, and the relaxation time, λ, extracted from the analysis of the temporal correlation functions against the extracted length scale, d, for the measurements performed using XMCD. Panels (c) and (d) shows the same analysis for the measurements performed using XMLD. There is no clear correlation between either β or λ on d for any of the measurement sets here.

consistent with those presented in the main body of the text. After being analysed in the same way as those in the main document, the extracted values of $\ln(K)$ are plotted against $\ln|1 - T_{\mathrm{Eff}}/T_{\mathrm{M}}|$ in Fig. 6 for measurements performed whilst both heating (panel (a)) and cooling (panel (b)). In conjunction with the critical slowing down model presented in the main text, a linear fit is applied to extract the critical scaling exponent, zv, for each data set, the results of which are presented in Table II. Critical speeding up is observed for all data sets here.

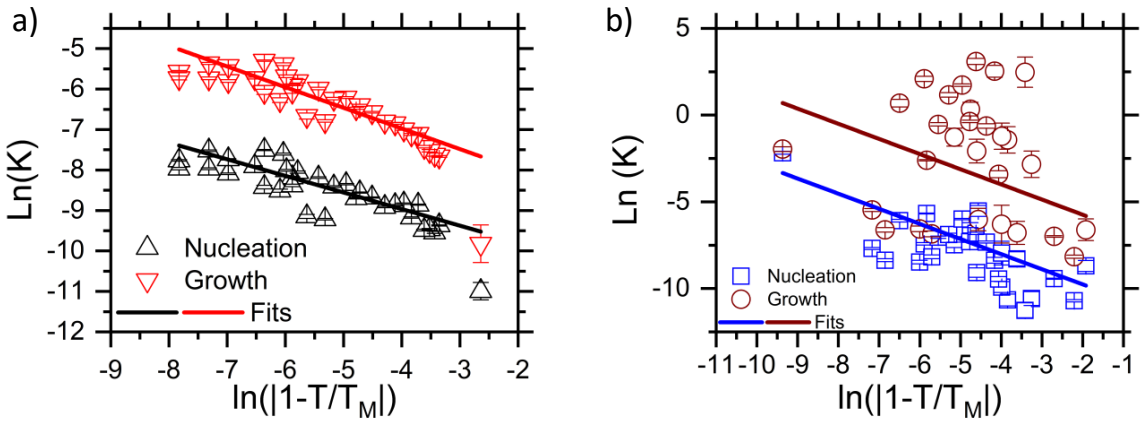

FIG. 6. Results of Avrami analysis for magnetometer based magnetic viscosity measurements performed under varying conditions. Panel (a) shows the values of $\ln(K)$ extracted for fits to measurements performed when heating, for both the nucleation and growth regimes, plotted against $\ln|1 - T_{\mathrm{Eff}}/T_{\mathrm{M}}|$. Panel (b) shows the same quantities extracted from the fits to measurements performed when cooling. The solid lines in these figures show linear fits in conjunction with the critical slowing down model presented in the main text. All data sets here present evidence of critical speeding up.

BEHAVIOUR OF THE AVRAMI EXPONENT

The Avrami analysis shown in the main body of the text contains a constant, n, which is known as the Avrami constant [8]. The extracted value of n for both the nucleation (N) and growth (G) phases of the dynamic behaviour is shown for all measurements presented in the main body of the text in Fig. 7(a) and (b) respectively. The extracted values of

TABLE II. Results of critical scaling exponent, zv, extracted by fitting of the critical slowing down model to the magnetometer based magnetic viscosity measurements taken in the absence of magnetic field.

	Nucleation	Growth
Heating	$-(0.41 \pm 0.04)$	$-(0.51 \pm 0.04)$
Cooling	$-(0.9 \pm 0.1)$	$-(0.9 \pm 0.3)$

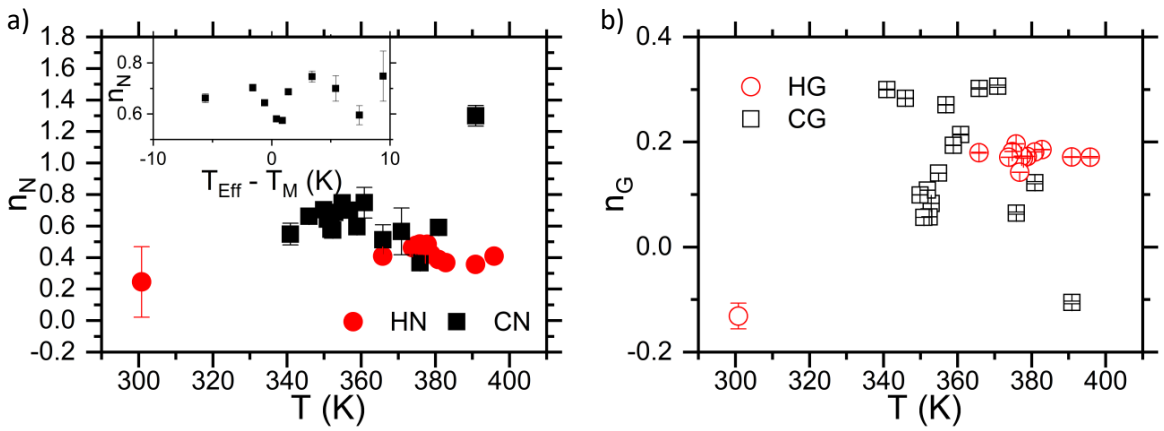

FIG. 7. Behaviour of the Avrami exponent through the transition. Panel (a) shows the behaviour of the Avrami exponent, n, extracted for the measurements performed using a magnetometer presented in the main body of the work for the nucleation (N) regime. The inset in panel (a) shows the behaviour of n centered around the transition midpoint, T_{M}. Panel (b) shows the same quantities but extracted from the fits to the growth regime. Red points show measurements performed when heating whilst black points are used to show measurements when cooling. All measurement sets performed when cooling see a variation in the extracted value of n for $T_{\mathrm{Eff}} \sim T_{\mathrm{M}}$. There is no obvious change around this temperature for measurements performed when heating.

n are typically between 0 and 1 and appear to vary again around the transition midpoint for all measurement sets apart from the growth phase when heating. The cooling branch measurements see the value of n decrease for $T \sim T_{\mathrm{M}}$ for both types of phase kinetics here, whilst the heating branch measurements see no obvious change over the measurement range for both phases of the dynamics.

The Avrami exponent is linked to the number of dimensions in which the changes within the sample take place [8, 9]. Avrami exponents of less than 1 have been attributed to the influence of more than characteristic relaxation time for a given kinetic process [9]. The change in the value of n approaching T_{M} then implies that the number of relaxation times changes at this temperature. This is likely to be due to the reduction in the relative energy barrier approaching this temperature and the distribution of transition temperatures through the film giving rise to a number of different environments each with their own kinetic properties.

DYNAMIC INVESTIGATIONS THROUGH THE SECOND-ORDER FERROMAGNET TO PARAMAGNET PHASE TRANSITION AT THE CURIE TEMPERATURE

Further to the investigations focused on the behaviour of the system in proximity to the first-order transition (FOPT) temperature presented in the main body of this work, similar investigations were also performed through the second-order phase transition (SOPT) taking place at the Curie temperature, T_{C}. These were performed in the magnetometer in an externally applied field of 0.1 T. Due to the fragility of the sample used in the XPCS experiments these investigations are performed on a different 60 nm thick FeRh sample which is grown on MgO. The temperature dependent magnetization profile of the sample taken between 300-700 K is shown in Fig. 8(a) and shows a FOPT between 300-450 K, as well as a SOPT around 670 K. To identify the exact position of T_{C}, the data between 450 and 700 K is fitted to the following equation [10],

$$M = M_0\left(1 - \frac{T}{T_{\mathrm{C}}}\right)^{\beta}, \tag{3}$$

where M_0 is the magnetization at 0 K and β denotes the nature of the approach towards the SOPT. The fits here yield values of $\beta = 0.493 \pm 0.001$ and $\beta = 0.467 \pm 0.001$ for fits to the heating and cooling branches respectively, which gives reasonable agreement with the mean-field model as consistent with previous measurements [2]. The values of $T_{\mathrm{C}} = 669.6 \pm 0.1K$ and $T_{\mathrm{C}} = 671.8 \pm 0.1$ K were extracted for the heating and cooling branches respectively.

Again, performing the Avrami analysis on this system reveals two distinct regions where a linear relationship between $\ln(-\ln(1-\alpha))$ is observed as seen for the measurements performed at 684 K in Fig. 8(b), which is again attributed to the nucleation and growth of domains. The fits to the data for the two regions are shown by the solid lines in this figure. Fig. 8(c) shows the behaviour of $\ln(K)$ extracted from the Avrami analysis for the measurements performed when cooling through the SOPT against $\ln|1 - T/T_{\mathrm{C}}|$. Here, as all of the measurements are performed in the same applied field there is no need to correct the temperature. A weak dependence on the rate constant upon the proximity to T_{C} is seen here, with the values extracted when both heating and cooling towards the SOPT shown in the summary of extracted values of zv in the main text. Only one of the measurements (growth phase for heating) demonstrates a value of zv that is significantly different from 0

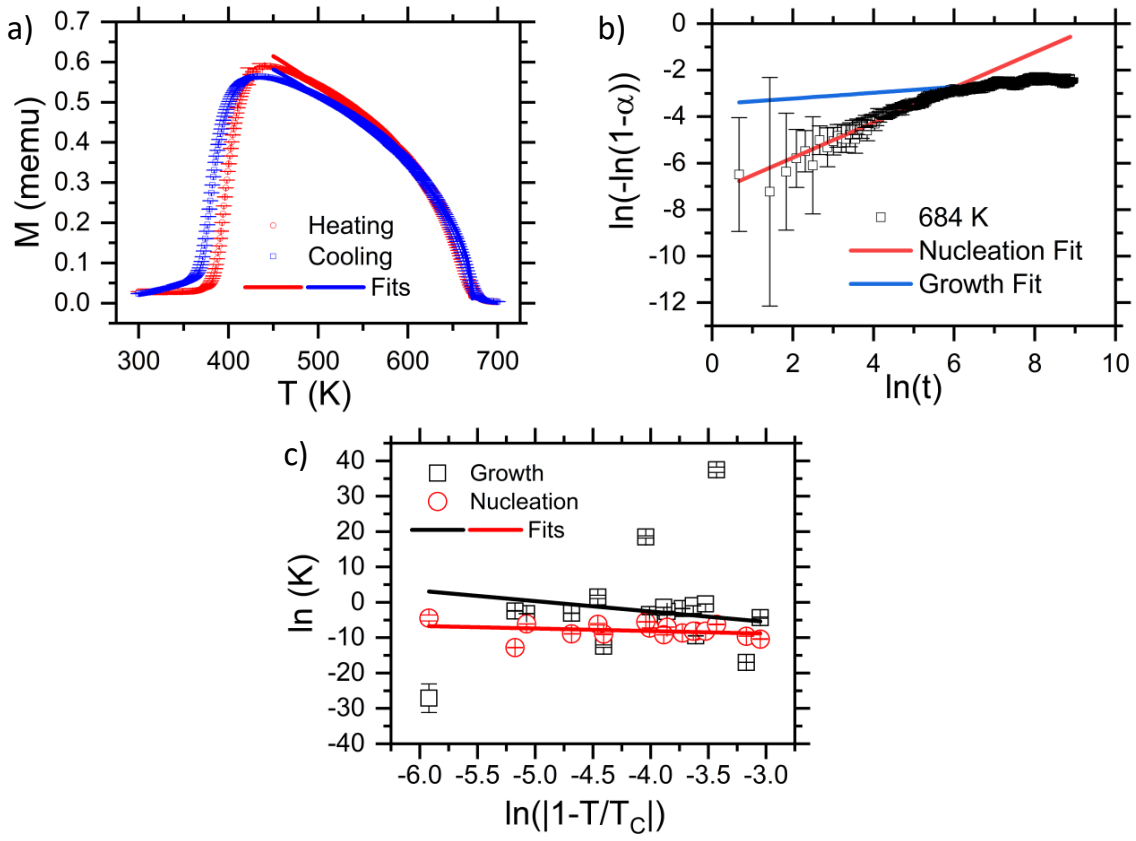

FIG. 8. Magnetometry based magnetic viscosity measurements through the second-order phase transition at the Curie temperature, T_{C}. Panel (a) shows the magnetization against temperature profile of a 60 nm FeRh sample grown on MgO between 300 - 700 K performed in a 0.1 T externally applied magnetic field. The blue points are those taken whilst cooling, and the red points are those taken when heating. Panel (b) shows examples of the Avrami analysis for a measurements performed at 684 K after cooling from 720 K. The solid lines show the fits for the two distinct regions of dynamic behaviour. Panel (c) shows the extracted values of $\ln(K)$ from the Avrami analysis plotted against $\ln|1 - T/T_{\mathrm{C}}|$ for measurements performed when cooling through the second-order phase transition at T_{C}. A weak dependence on the proximity to the phase transition is seen here.

within a 95% confidence level.

[1] Maat, S., Thiele, J. U. & Fullerton, E. E. Temperature and field hysteresis of the antiferromagnetic-to-ferromagnetic phase transition in epitaxial FeRh films. *Phys. Rev. B*

72, 214432 (2005).

[2] Massey, J. R. *et al.* Phase boundary exchange coupling in the mixed magnetic phase regime of a pd-doped ferh epilayer. *Phys. Rev. Materials* **4**, 024403 (2020).

[3] Almeida, T. P. *et al.* Quantitative TEM imaging of the magnetostructural and phase transitions in FeRh thin film systems. *Sci. Rep.* **7**, 17835 (2017).

[4] Temple, R. C. *et al.* Antiferromagnetic-ferromagnetic phase domain development in nanopatterned FeRh islands. *Phys. Rev. Materials* **2**, 104406 (2018).

[5] Chen, S.-W. *et al.* Jamming behavior of domains in a spiral antiferromagnetic system. *Phys. Rev. Lett.* **110**, 217201 (2013).

[6] Djurberg, C. *et al.* Dynamics of an interacting particle system: Evidence of critical slowing down. *Phys. Rev. Lett.* **79**, 5154 (1997).

[7] Morley, S. A. *et al.* Vogel-Fulcher-Tammann freezing of a thermally fluctuating artificial spin ice probed by x-ray photon correlation spectroscopy. *Phys. Rev. B* **95**, 104422 (2017).

[8] Loving, M. *Understanding the Magnetostructural Transformation in FeRh thin films.* Ph.D. thesis, The Department of Chemical Engineering, Northeastern University (2013).

[9] Lin, F. X., Zhang, Y. B., Tao, N., Pantleon, W. & Jensen, D. J. Effects of heterogeneity on recrystallization kinetics of nanocrystalline copper prepared by dynamic plastic deformation. *Acta Materialia* **72**, 252 (2014).

[10] Blundell, S. *Magnetism in Condensed Matter*, chap. 6 (Oxford University Press, 2001).